TECHNISCHE UNIVERSITÄT DRESDEN

Faculty of Computer Science Institute of Artificial Intelligence

TUD-FI16-02 September 2016

Quantification and Classification of Cortical Perfusion during Ischemic Strokes by Intraoperative Thermal Imaging

Nico Hoffmann, Georg Drache, Edmund Koch, Gerald Steiner, Matthias Kirsch and Uwe Petersohn

Technische Berichte
Technical Reports
ISSN 1430-211X

Technische Universität Dresden
Faculty of Computer Science
D-01062 Dresden
Germany

Quantification and Classification of Cortical Perfusion during Ischemic Strokes by Intraoperative Thermal Imaging

Nico Hoffmann*, Georg Drache*, Edmund Koch†, Gerald Steiner†, Matthias Kirsch‡§¶ and Uwe Petersohn*
*Applied Knowledge Representation and Reasoning, Faculty of Computer Science,Technische Universität Dresden, Dresden, Germany
†Clinical Sensoring and Monitoring, Faculty of Medicine Carl Gustav Carus, Technische Universität Dresden, Dresden, Germany
‡Neurosurgery, University Hospital Carl Gustav Carus, Technische Universität Dresden, Dresden, Germany
§CRTD/DFG-Center for Regenerative Therapies Dresden Cluster of Excellence, Technische Universität Dresden, Dresden, Germany
¶Nationales Centrum für Tumorerkrankungen (NCT), Dresden, Germany

***Abstract*—Thermal imaging is a non-invasive and marker-free approach for intraoperative measurements of small temperature variations. In this work, we demonstrate the abilities of active dynamic thermal imaging for analysis of tissue perfusion state in case of cerebral ischemia. For this purpose, a NaCl irrigation is applied to the exposed cortex during hemicraniectomy. The cortical temperature changes are measured by a thermal imaging system and the thermal signal is recognized by a novel machine learning framework. Subsequent tissue heating is then approximated by a double exponential function to estimate tissue temperature decay constants. These constants allow us to characterize tissue with respect to its dynamic thermal properties. Using a Gaussian mixture model we show the correlation of these estimated parameters with infarct demarcations of post-operative CT. This novel scheme yields a standardized representation of cortical thermodynamic properties and might guide further research regarding specific intraoperative diagnostics.**

I. Introduction

Ischemic strokes denote the shortage of substrates of delimited areas of the brain by a blockage of vessels (embolism or thrombosis). Severe strokes lead to a swelling of brain tissue, which raises the intracranial pressure (ICP) yielding a bad or fatal prognosis if not treated appropriately. Hemicraniectomy can be considered as last resort to decrease the ICP.

In brain tissue, temperature variations are primarily caused by heat transfers originating from cerebral perfusion. In fact, the local cerebral blood flow correlates with cell metabolism and can be used as marker for tissue state and neural activity. Intraoperative thermal imaging now allows the inference of diagnostic information about perfusion- and neural activity related disorders. In general, thermal imaging is a contactless, marker-free, white-light independent and non-invasive method for online measurement of temperature variations up to $30\ \mu K$. Current uncooled devices use infrared microbolometer focal plane array detectors measuring a field of view of 16 x 12 cm with an underlying spatial resolution of $250\ \mu m$ per pixel at a framerate of 50 Hz. The detected infrared radiation arriving at the microbolometer array is processed and stored as two-dimensional image.

In the past, Gorbach et al. provided a method to distinguished tumor tissue from normal tissue based on thermal imaging[1]. Additionally, Steiner et al. visualized the cortical blood flow by analyzing the spatial distribution of a cold bolus applied through a central line with multivariate analysis tools[2].

In this work, we propose an alternative approach to the cold bolus method of Steiner et al. in order to characterize the perfusion state of cortical tissue. In general, we describe a machine learning framework to recognize cortical irrigations. Furthermore, a mathematical model is designed such that it allows us to quantify the time-dependent thermal behavior during the treatment of ischemic strokes. The proposed method allows the selective analysis of cortical tissue and integrates seamlessly into current intraoperative workflows. In contrast to the cold bolus approach, our method is not limited to perfused areas and provides us to control the signal-to-noise ratio of our target pattern. Finally, we extend prior findings of Gorbach et al.[3] by a straightforward intraoperative approach with a sound mathematical approximation of the time-dependent behavior of cortical tissue.

II. Related Work

In the last years, sensor technology for uncooled thermal imaging has developed in terms of accuracy. This enables a wide range of applications for thermal imaging. Branemark et al. found that diabetes correlates with reduced body temperatures[4]. These findings were supplemented by Sun et al. who investigated the thermal behavior of human extremities under diabetes. They found a significantly elevated average temperature of the human feet which might be a marker for early diabetic neuropathy[5].

Blood pressure monitoring as discussed by Cesaris et al. is another possible application field of thermal imaging[6]. Thermography was even employed in the field of dentistry[7]. Since fever typically leads to an increased face temperature, it was shown that thermal imaging can be used to recognize SARS [8].

Active dynamic thermography depicts an approach that requires the utilization of a temperature gradient to a surface in

order to inspect its structures. Since heat transfers propagate into the depth of an object, varying the amplitude of the temperature gradient allows inspecting different object layers and thereby enables some sort of thermal tomography[9]. This idea was also brought into medical domain. Deng and Liu[10] evaporated a 75% ethanol solution on tissue and found that it might be an indicator for subsurface breast cancer. Gorbach et al.[3] irrigated the exposed cerebral cortex with ice cold saline solution for two seconds. He then recorded the temperature increase and found that tumor tissue took more time to reach the equilibrium temperature compared to healthy tissue. He concluded dynamic thermal imaging might be suitable for the analysis of tissue displacement during surgery.
In this wor, we contribute an approach that integrates seamlessly into intraoperative workflows and a sound mathematical framework to get a standardized representation of tissue heating behavior. The approach doesn't require any external input of surgical personal for the detection of irrigation events and subsequent visualization of the results.

III. Materials and Methods

Gorbach et al. proposed irrigating the surface of cortical tissue for some time to propagate heat through several tissue layers[3]. In contrast, we employ available intraoperative tools to prevent the need for additional sterile tools. The surgeon typically has a tool (e.g. syringe) to purge sterile sodium chloride (NaCl) onto tissue. Hereby, it is possible to selectively apply NaCl to a delimited area of the exposed cortex for a specific duration.
This irrigation induces a steep drop in temperature followed by a temperature increase caused by heat transfers. In human tissue, this heating correlates with thermodynamic properties of the underlying tissue, thermal conductivity and tissue perfusion state. By modeling this behavior and estimating respective parameters, it is possible to characterize the imaged tissue.

A. Approximation of Dynamic Thermal behavior

In 1948, Pennes[11] proposed the biologically inspired "Bioheat equation". He proposed the following model to describe internal as well as external influences to the heat distribution in living tissue:

$$c_p \rho \frac{\delta T(x,y,z)}{\delta t} = \kappa \nabla^2 T(x,y,z,t) + q_b + q_m + q_{ex} \quad (1)$$

with the specific heat c_p, material density ρ, the temperature distribution $T(x,y,z)$ at time t $T(x,y,z,t)$ and thermal inductivity κ. He further added biological parameters describing the heat power density of q_b blood flow, q_m metabolism and external power density q_{ex}.
Several authors have shown the discretization of Penne's equation (see for example Gutierrez et al.[12]). In our case, we are facing several a priori unknown parameters, whose estimation schemes would introduce significant computational complexity and potentially inaccurate estimates. To counter these challenges, we employ Nowakowski's approach to approximate tissue's thermal behavior by a double exponential function[13]:

$$T(t) = T_{equ} + \Delta T_1 exp(-t\lambda_1) + \Delta T_2 exp(-t\lambda_2) \quad (2)$$

In this equation, T_{equ} represents the tissue's equilibrium temperature, ΔT_1 and ΔT_2 are the scaling coefficients of both exponential functions. The decay constants λ_1 and λ_2 with unit s^{-1} represent the amplitude of the tissue's temperature change rate. This model approximates the tissue heating following the application of a cold cortical irrigation with NaCl. Hereby, we are able to quantify the cortical perfusion as it correlates with the rate of temperature change.
By application of a liquid to the exposed cortex, we expect to observe at least two different components that are well described by this double exponential function. One component represents the temperature changes of the applied cool fluid. The other component describes the temperature change of the affected underlying tissue. The latter dominates the temperature change after the fluid drained from the surface. The elevated ICP in case of cerebral ischemia results in the cortex having a convex shape with high curvature. Therefore, we expect the applied fluid to drain continuously. This means that λ_1 of the fluid is larger than the temperature rise, λ_2, of the underlying tissue yielding a reliable estimate of λ_2. However, it is essential to apply a significant temperature gradient to the cortex for accurate parameter estimation, otherwise the dynamic temperature behavior caused by the draining NaCl solution can't be differentiated from tissue heating. This would prevent any subsequent analysis based on λ_2.
Two factors affect the accuracy of the proposed method: the temperature difference between liquid and cortex and the application time of the fluid before its drainage.
A high curvature of the cortex leads to a fast fluid drain and low irrigation impact requiring longer application times. Also, an accumulation of fluid is to be prevented since this would hamper any reliable estimate of λ_2. Note that the model applies to single time series, what allows for heterogeneous application pattern of the liquid - as long as ΔT_2 is maximized.

B. Irrigation Detector

The potential heterogeneous selective irrigation of specific parts of the exposed cortical surface requires to unveil all timepoints of irrigation events for each pixel in order to analyse its dynamic thermal behavior.
This recognition task is difficult because of the variety of irrigation patterns, the caused temperature decrease can also be very low and hard to distinguish from background noise. In order to solve these issues, we propose a framework consisting of three steps (see Fig. 1):

1) Irrigation Window Determination
2) Spatial Scoring
3) Warming Period Detection

The first step depicts a fast approximate search for possible irrigation events. Afterwards, the events are correlated with events of adjacent pixels to improve detection accuracy. In a

last step, a main irrigation event is estimated for subsequent heating analysis given our double exponential model.

1) Irrigation Window Determination: An irrigation event denotes the whole time frame when a cold liquid is being applied to the exposed cortex. This irrigation event causes a rapid change in temperature followed by a slow temperature rise. Since we aim to analyze the heating behavior following an irrigation, we have to estimate a precise irrigation timestamp. In order to improve the speed of this process, we employ a hierarchical estimation scheme. First, the stream of thermal images is partitioned into overlapping windows that can be analyzed independently. In the following, we omit additional notations for the respective window as it can be achieved by partitioning timestamps t_i respectively. In order to detect the irrigations efficiently, we exploit that an irrigation event causes a steep temperature decrease and a slow increase to the tissue's equilibrium temperature. This behavior introduces a characteristic pattern into the sorted temperature series $s(p, t_i)$ (see fig. 2). Since the irrigation pattern can be recognized in the lower temperature part of the sorted time series, no additional template matching is necessary. This means that we can analyze all pixel's timeseries at once.

Let $s(p, i)$ denote the time points of the sorted temperature series of pixel $p \in \mathbb{N}^2$ with index $i \in [1, .., n]$ given n measurements. For each $s(p, i)$ there is an $t_j(p)$ with $j \in [1, .., n]$ such that $T(p, s_i(p)) = T(p, t_j(p))$. By $T(p, t_i(p))$ we denote the i-th measured temperature of pixel p at time $t_i(p)$. For reasons of comprehensibility, we omit the pixel index p when not necessary. In general, an irrigation event is recognized by evaluating the following equation:

$$m(p) = f_{\text{norm}} \times \sum_{i=i_1}^{i_{step}} |T(p, s_i(p)) - corr(i)| < \mathrm{t_{div}} \quad (3)$$

given normalization constant f_{norm}, threshold $\mathrm{t_{div}}$ and a correlation function $corr(\cdot)$. The index variables i_1 and i_{step} represent the heating window. Those constants are explained in the following paragraphs. The latter computes the similarity of the measured temperature to our model function by a single exponential function. This idea is similar to the shapelet approach of Ye and Keogh[14]). The correlation function is defined by

$$corr(t) = lim_{up} - (lim_{up} - lim_{bottom}) exp(-\lambda(t - t_{start})) \quad (4)$$

with t_{start} being short for $s_{i_{start}}$. The parameters are approximated from the sorted timeseries by

$$lim_{up} = T(s(i_{step})) + 0.1 \quad (5)$$

$$lim_{bottom} = T(s_{i_{start}})) \quad (6)$$

$$\lambda = n^{-1} \sum_{i=1}^{n} \left\{ -n^{-1} ln \left(\frac{lim_{up} - T(s_{z_i}))}{lim_{up} - lim_{bottom}} \right) \right\} \quad (7)$$

at a certain number of supporting points n. By i_{step}, we denote the position of the step or last frame of the regarded irrigation window while i_{start} denotes the index of the first frame. The upper limit (lim_{up}) of the exponential decay function is set to the temperature $T(t_{step})$ representing the highest temperature after the irrigation event. A margin of $.1K$ is added to avoid divisions by zero. The lower limit (lim_{bottom}) corresponds to the lowest temperature in our window. A rough estimate of the decay constant λ is computed at three supporting points z_i. For each z_i, we estimate λ and solve the consensus problem by simply averaging all three estimates. This scheme yields a fast approximation of the characteristic warming behavior. We have to emphasize that this method is employed as first step to the recognition of our heating pattern, in subsequent steps we estimate the parameters of our proposed model (see section III-A) by a robust method.

2) Spatial Scoring: Irrigations typically affect multiple adjacent pixels with similar temperature gradients. In the following, we discuss an approach to account for this effect and thereby improve overall accuracy of our irrigation detector framework. Spatial scoring denotes that we use the information of adjacent irrigation events when reasoning about local irrigation events. This means that the score correlates with spatial homogeneity and similarity of irrigation events. A clear similarity leads to a high score value for all affected pixels. In general, the score σ of pixels p_s and p_t is defined by

$$\sigma(p_s, p_t) = f \times max(\Delta T_{p_s}, \Delta T_{p_t}) \quad (8)$$

with $\Delta T = \underset{i \in I}{max}\ T(i) - \underset{j \in I}{min}\ T(j)$ and I being the set of all indexes of the analyzed window. ΔT is therefore defined as maximal temperature deviation. Let further be

$$f(p_s, p_t) = \begin{cases} 0, & \text{no irrigation} \\ f_m(p_s, p_t), & \text{irrigation at } p_s \text{ or } p_t \\ 2f_m(p_s, p_t), & \text{irrigation at both sites} \end{cases} \quad (9)$$

and

$$f_m(p_s, p_t) = \begin{cases} \nu_1, & \Delta t_m(p_s, p_t) < t_{m_1} \\ \nu_2, & t_{m_1} \leq \Delta t_m(p_s, p_t) < t_{m_2} \\ \nu_3, & t_{m_2} \leq \Delta t_m(p_s, p_t) < t_{m_3} \\ 0, & t_{m_3} < \Delta t_m(p_s, p_t) \end{cases} \quad (10)$$

t_{m_i} and ν_i with $i \in [0; 3]$ are penalty parameters. By $\Delta t_m(p_s, p_t) = min(|ts_{p_s}(i) - ts_{p_t}(j)|)$ we denote the minimal temporal distance of the minimum temperature of two pixels p_s and p_t, whereas ts are lists of timestamps of the k lowest temperatures in the evaluated interval. The score (equation 8) represents the assumption that neighboring pixels are affected by an irrigation event at little temporal difference. In order to compute a weighted score by including the neighbors $\mathcal{N}(p)$ of pixel p, we have

$$\sigma(p_s)^{sum} = \sum_{p_t \in \mathcal{N}(p_s)} \Delta(p_s, p_t) \times \sigma(p_s, p_t) \quad (11)$$

wherein $\Delta(p_s, p_t) = 1/(ln||p_s - p_t||_2 + 1)$ is a distance metric depending on the spatial position of pixels p_s and p_t. Therefore, $\sigma(x)^{sum}$ is a weighted sum of neighboring scores. An irrigation event is flagged as detected, if the following holds

$$f^{detect} = \begin{cases} 1, & \sigma^{sum} \geq H \times t_f \\ 0, & otherwise \end{cases} \quad (12)$$

with H being the highest score reached during analysis capped to minimum level σ_{ref}: $H = min(\max_{p_s,p_t \in I}(\sigma(p_s,p_t)), \sigma_{ref})$.

3) Warming Period Detection: The preceding steps yield a list of irrigation events. For reasons of comparison, we propose to evaluate only warming phases caused by the same irrigation event. Ideally, the liquid is applied instantaneously to the whole surface leading to very similar irrigation events. However, the propagation of temperature gradient into deeper tissue layers requires a slow, circular application of the liquid. This leads to many irrigation events originating from a global liquid application with spatially-dependent timestamps.
The time point of the global liquid application is denoted by irrigation reference and has to be recovered. Let $h(t_j)$ be the number of pixels with an irrigation event at timestamp t_j. The set $\mathbb{C}$ denotes the set of all possible irrigation timestamps. The reference timestamp t_{ref} is estimated as of

$$t_{ref} = \underset{t_j \in \mathbb{C}}{argmax} \left\{ \sum_{i=-2}^{i=2} h(t_{j+i}) \right\} \tag{13}$$

The latter equation recovers the timestamp of a reference irrigation event by evaluating the number of pixels being affected by an irrigation within 5 consecutive frames.
By fixing t_{ref}, we recover all pixels belonging to this reference irrigation. Therefore, an irrigation event at pixel i to t_{ref} is accepted if it occurred ± 5 seconds with respect to the reference timestamp. The recovered timestamp of pixel p_s is denoted by $t^*(p_s)$. Reliable model parameter estimates are achieved by evaluating the pixel's score at t^* while omitting irrigation events with weak score.

4) Parameter Learning: The proposed framework consists of several parameters for a fast and reliable detection of irrigation events. In order to improve the accuracy of our irrigation detector and adopt it to characteristics of the discussed use case, we learn relevant parameters from training data. The parameters have to be learned once and can then be used in subsequent intraoperative measurements. For parameter learning, we employ a Markov Chain Monte Carlo (MCMC)[15] sampler that we will discuss now.
Markov Chain Monte Carlo methods draw dependent samples of a probability distribution. Each drawn sample fulfills the local Markov property meaning that it only depends on the previously drawn sample and a given probability distribution. The Metropolis-Hasting MCMC sampler is a canonical approach based on three main steps for drawing and accepting some sample θ:

1) draw θ^t from proposal distribution $p(\theta^t; \theta^{t-1})$
2) compute acceptance probability $p(\theta)$
3) accept if $p(\theta)$ is sufficiently large

The proposal distribution is modeled as normal distribution such that $p(\theta^t; \theta^{t+1}) \sim N(\theta^{t+1}, \sigma)$ given σ describing the step length. The overall energy of a configuration θ is denoted by

$$f(\theta) = \sqrt{f_{pos}^2 + f_{neg}^2} \tag{14}$$

with f_{pos} being the number of false positives and f_{neg} being the number of false negatives of the irrigation detector.
Since we only want to evaluate the latest irrigation event, i.e. the event being followed by a temperature increase until equilibrium temperature, we have to adopt the learning strategy for the multiple irrigation event detector. Suppose the warming behavior can be approximated by a double exponential function, then we arrive at the energy function of configuration θ for the multiple irrigation event detector

$$f(\theta) = \min_{\theta} \left\{ \sum_i \sum_{t=0}^{5s} |T_i(t) - \widetilde{T}_i(t)| \right\} \tag{15}$$

with $\widetilde{T}$ being the fitted double exponential function as of equation 2. By this formulation, we can quantify the divergence of expected non-linear warming behavior and the measured one after the estimated irrigation event. Note that the upper limit of $5\ s$ is an empirical constant requiring that the warming time must be at least 5 seconds.
Since the parameters of the single irrigation event detector are independent of multiple event detector's parameters, we first estimate the parameters for the single detector and afterwards for the multiple irrigation detector. The modified MH-sampler given an arbitrary configuration θ is sketched by algorithm 1.

Algorithm 1: MH-sampler to learn parameters of the discussed irrigation detection and tissue classification framework.

input: step width σ
input: number of iterations l
input: tolerance ϵ
output: parameter vector $\theta^* \in \mathbb{R}^k$

randomly sample $\theta_1 \in \mathbb{R}^k$*;*
for *iteration* $t \leftarrow 1$ **to** l **do**
  randomly choose dimension i *of* $(1;k)$ *;*
  sample $\theta_i^{t+1} \sim N(\theta_i^t, \sigma)$ *;*
  accept θ_i^{t+1} *if* $f(\theta^{t+1}) < f(\theta^t)$ *or if*
  $p_{acc}(\theta^{t+1}, \theta^t) = \frac{f(\theta^t)^2}{f(\theta^{t+1})^2}$ *is sufficiently small.;*
  if $f(\theta^{t+1}) < \epsilon$ **then**
    stop;

C. Classification

As discussed, the temperature decay parameter λ_2 describes the heating behavior of underlying tissue. In case of an ischemic stroke, we further expect low values of λ_2 in under- or unperfused tissue. The parameter λ_2 should be significantly larger in healthy areas due to high perfusion and metabolism in living tissue. We also hypothesize characteristic behavior in-between healthy and ischemic tissue what we denote by "uncertain".
Therefore λ_2 is partitioned into tissue states $\mathbb{S} = \{ischemic, uncertain, healthy\}$. λ_2 is expected to vary in

each state at different scales. Therefore, we model the expected behavior of the temperature decay constant λ_2 by the following Gaussian mixture model:

$$\lambda_2^{ischemic} \sim N(\mu_i, \sigma_i)$$
$$\lambda_2^{uncertain} \sim N(\mu_u, \sigma_u)$$
$$\lambda_2^{healthy} \sim N(\mu_h, \sigma_h)$$

Since the parameters $\Theta = (\mu_i, \mu_u, \mu_h, \sigma_i, \sigma_u, \sigma_h)$ of each class are patient specific and a priori unknown, we propose to employ the EM algorithm for parameter estimation. Its actual derivation can be found elsewhere (see for example Bishop[16]).
For each λ_2, this model yields the probabilities $p(y|\lambda_2; \Theta)$ of belonging to state $s \in \mathbb{S}$. At specific pixel location p, we are now able to infer the most probable tissue state

$$\widetilde{s}_p \in \underset{s_p \in \mathbb{S}}{argmax}\ p(s_p|\lambda_2(p); \Theta) \tag{16}$$

Each state's probability might be a reasonable indicator to infer further knowledge regarding the possible future progression of the ischemic demarcation.

D. Overview of the Irrigation detection and classification scheme

The proposed framework consists of several steps for detection of irrigation events, feature extraction and classification. Algorithm 2 shows the whole algorithm.

Algorithm 2: Schematic overview of the proposed irrigation detection and tissue classification framework.

input: data set, $T \in \mathbb{R}^{n \times m}$
input: parameter vector, $\theta \in \mathbb{R}^l$
output: classified image, $X^* \in \mathbb{R}^n$

for *pixel* $k \leftarrow 1$ **to** n *and window* w **do**
  sort timeseries $T_{(k,w)} \rightarrow s_{(k,w)}$;
  if *m(k) = False* **then**
    skip w;
  $f^{detect}_{(k,w)} = \sigma^{sum}_{(k,w)} > H \times t_f$;
compute histogram $h(f^{detect})$;
recover $t_{ref} = \underset{t_j \in \mathbb{C}}{argmax} \left\{ \sum_{i=-2}^{i=2} h(t_{j+i}) \right\}$;
find $p \in \mathbb{P}$ *with irrigation events* $|t_p^* - t_{ref}| \leq 5s$;
solve eqn. 2 for $t^* \leq t \leq t^* + 5s$;
classify decay constant $\lambda_2(p)$ *by a 3-GMM;*

IV. Results and Discussion

We performed several experiments to evaluate the performance of the proposed irrigation event detector. All intraoperative procedures were approved by the Human Ethics Committee of the Technische Universität Dresden (no. EK 323122008). Informed consent was obtained postoperatively in accordance with the approved scheme.
In the following, we evaluate the detector's performance in experimental test and training datasets. These are also used for learning the parameter configuration of the detectors. Afterwards, the approach is used to analyze intraoperative data.

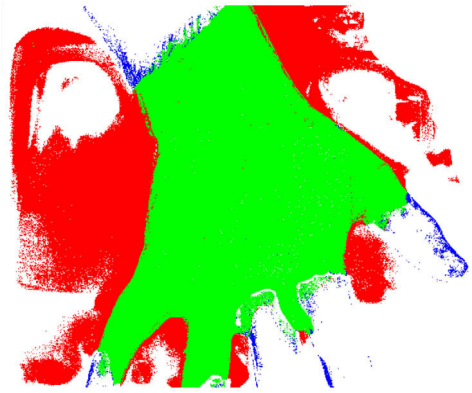

Fig. 3. The detected irrigations of dataset "20, hand pour" strongly deviate from the results of other test datasets. After application of the temperature gradient to the hand, the liquid drained into a water basin beneath the hand. This behavior resembled a typical irrigation and was detected by the proposed framework. Green resembles a true positive, blue a false negative and red a false positive classification.

A. Evaluation Datasets

It is fairly difficult to simulate the thermal behavior of the cortex experimentally since well-perfused exposed cortical tissue is necessary. Therefore we chose to measure the temperature propagation of the arm and hand of a volunteer as phantom. Both parts of the body also have near-surface vessels, comparable curvature, are quite homogeneously perfused but do not contain any hotspots or underperfusion. The surface temperature was approximately $28\ ^\circ C$. We applied several temperature gradients to the surface: $\{-8, -3, 0\}$ K whilst measuring thermal data of the surface.
We discovered two different styles of applying the irrigation liquid during intraoperative measurements: pour method and spray method. Pour implies that all of the liquid is applied to the cortex at once meaning that all the affected tissue is cooled down simultaneously. The spray method is a more flexible approach. Hereby the surgeon applies a jet of the NaCl solution to the surface in a circular manner. This can be repeated several times leading to multiple irrigation events and resulting in a very heterogeneous fluid distribution on the surface. Yet, the spray method allows a deeper propagation of temperature gradients. We simulated both behaviors during our experiments. The experimental setup consisted of a volunteer placing his hand over a glass basin. Then, water was applied to the hand in order to cause a heat transfer and subsequently drained off into the basin.

B. Irrigation Detector

The evaluation datasets were partitioned into training and test datasets. Using the MCMC sampler, the parameters t_f (see

Dataset	Accuracy [%]	False Negative [%]	False Positive [%]
-8, h-spr-r	88.7	3.7	7.6
-8, h-pour	80	1.5	18.5
-3, h-spr-r	95.1	3.1	1.8
-3, h-pour	97.5	1.7	0.8
0, h-spr-r	95.9	3.4	0.7
0, h-pour	97.6	1.9	0.5
no irrigation, h	98.6	0.0	1.4

TABLE I

THIS TABLE LISTS THE PERFORMANCE OF THE PROPOSED IRRIGATION DETECTOR FRAMEWORK ON APPLIED IRRIGATIONS ON THE HAND SURFACE.

eqn. 3) and divergence threshold (see eqn. 8) were learned. The sampler achieved acceptance rates ranging from 85 % to 92 %. The results further indicate the detector achieves a good overall accuracy (see table I). We further observe a great margin in parameter space since many parameter configurations seem to perform equally well given the training and test data. The performance of $-8h-spr-r$ and $-8h-pour$ dataset deviate significantly from other results in terms of false positives (see figure 3). We found that this raised false positive rate is caused by the experimental setup. Both datasets were recorded during the first experimental run, so that the former dry and warm basin got cooled down by the fluid triggering a cooling detection. In latter runs, we filled the basin with a small amount of water to prevent this issue.

C. Tissue Characterization

Prior to the following analysis and discussion we want to emphasize that the cortical temperature distribution in case of cerebral ischemia hasn't been evaluated by thermal imaging before. Therefore we validated our model assumption regarding the differentiability of λ_1 and λ_2 empirically. As hypothesized, λ_1 is one order of magnitude larger than λ_1 because of the fast draining effect. The distribution of both parameters can be seen in figure 4.

In detail, the cohort contained cases of ischemic strokes of middle cerebral artery (MCA) respectively anterior cerebral artery (ACA) requiring a decompressive hemicraniectomy to decrease intracerebral pressure. Accompanying and without influencing the surgical intervention we performed thermographic measurements of the exposed cortex and recorded intraoperative irrigations. These irrigations are common in neurosurgery in order to prevent cortical drying.

It has to be emphasized that this intervention typically occurs in an emergency situation what prevents lengthy measurement procedures and complex experimental requirements. Therefore, we were not able to apply an irrigation liquid of appropriate temperature in some cases leading to less meaningful results.

In order to validate the results, we segmented the infarct demarcation in pre- and postoperative computed tomography (CT) scans. After image registration of intraoperative thermal imaging with these CT recordings, we were able to correlate the results. CT recordings are acquired at varying amount of hours before and after the intervention hampering the comparison with intraoperative results in some cases. It is synchronize to correlate the time of the CT recording with the time of the underlying ischemic stroke. The findings of the application of our detection and classification scheme to intraoperative data are summarized in table II. We classified the results into three categories: positive, questionable, and negative. The majority of our evaluated cases show a correlation (positive result) of the λ_2 segmentation with the infarct demarcation in CT (see Fig. 5 as one example of this class). Yet, in one case, we observed a questionable result, wherein the λ_2 segmentation reveals more healthy tissue than being seen in the CT recording. We suppose this outcome to correlate with tissue of uncertain state meaning that the healthy classified tissue might be in a state in-between alive and dead. Latter assumption require more research regarding the approximation of the uncertain state by our assumed $N(\mu_u, \sigma_u)$. We further observed two case (id 1 and 2) with negative outcome. In case 1, the liquid was applied by the pour approach. Due to the increased curvature of the exposed cortex caused by increased ICP, the fluid drained fast and didn't cause significant temperature propagations into deeper tissue layers. Therefore, no reliable λ_2 estimates could be achieved. Due to unknown thermodynamic and vascular effects, the exposed cortex at the infarct site in case 2 was colder than expected leading to the application of a too warm NaCl solution, which heated the cortex and did not impose any irrigation. Therefore, the detector couldn't recognize significant irrigations at certain sites (see Fig. 6). The other three 4 cases showed an evident correlation between the segmented temperature decay constant λ_2 and the infarct demarcation in CT measurements.

During our experiments, we encountered several challenges. In case of a low temperature gradient the estimated ΔT_2 of model equation 2 yielding potentially unreliable estimates of λ_2. Depending on the application of the liquid and the cortical curvature, it might not be possible to separate the drainage of fluid from tissue's warming process resulting in $\lambda_1 \approx \lambda_2$. Both challenges are primarily caused by high curvature or a too less amount of fluid being applied to the cortex. If the applied temperature gradient is too low, the tissue temperature returns to equilibrium temperature very fast. This prevents the projection of the temperature gradients into deeper tissue layers and prohibits adequate classification.

In general, the proposed irrigation detection framework achieved an accuracy of up to 97.6 %. This allowed us to

id	sex/age	pathology	result	comment
1	f/61	MCA infarct	negative	no temperature propagation due to increased ICP
2	f/61	MCA+ACA infarct	negative	liquid hotter than surface
3	m/59	MCA infarct	positive	
4	f/50	MCA infarct	questionable	to broad classification of healthy tissue
5	f/63	vasoplastic infarct	positive	
6	f/75	MCA infarct	positive	

TABLE II
OVERVIEW OF RESULTS FROM CLASSIFYING THE DECAY CONSTANT OF TISSUE HEATING AFTER APPLICATION OF AN INTRAOPERATIVE IRRIGATION TO THE CORTEX.

estimate the parameters of discussed dynamic tissue temperature model. Hereby, we are able to quantify standardized thermodynamic properties of imaged tissue allowing conclusions regarding its perfusion state.

V. SUMMARY

Thermography is an emerging whitelight-independent, non-invasive method to measure the temperature distribution of surfaces. Active dynamic thermography allows us to quantify dynamic thermal behaviour by the application of temperature gradients. In the medical domain, this enables the detection of abnormal tissue and vascular pathologies.

In this study, we employ active dynamic thermography in order to analyze the perfusion of the exposed human cortex during neurosurgical interventions in case of ischemic strokes. The proposed method requires the application of a temperature gradient to the exposed cerebral cortex in order to recover information regarding its perfusion state. Temperature gradients are introduced by the application of cold NaCl irrigations to the surface of the exposed cortex. These events are imaged and detected by a novel online machine learning framework. Following this, the tissue perfusion can be approximated by the estimation of the parameters of the discussed perfusion model. Its parameters include thermal decay constants that quantify the heating behavior of tissue.

We were the first to show that the intraoperative segmentation of temperature decay constants by a 3-Gaussian mixture model correlates with preoperative infarct demarcations in CT imaging. This enables the surgeon to recognize the progression of infarct demarcations from preoperative measurements to the actual intraoperative scene. Further research has to be done in order to improve the clinical significance of our results by an extensive validation study and advance the predictions of the machine learning framework. The estimated parameters yield a standardized representation of cortical perfusion meaning that the accuracy might be advanced by applying supervised learning.

VI. ACKNOWLEDGEMENT

This work was supported by the European Social Fund (grant no. 100087783). The authors would also like to thank all other organizations and individuals, especially the surgical and nursing staff, that supported this research project.

REFERENCES

[1] A. M. Gorbach, J. D. Heiss, L. Kopylev, and E. H. Oldfield, "Intraoperative infrared imaging of brain tumors," *Journal of Neurosurgery*, vol. 101, no. 6, pp. 960–969, 2004, pMID: 15599965. [Online]. Available: http://thejns.org/doi/abs/10.3171/jns.2004.101.6.0960

[2] G. Steiner, S. B. Sobottka, E. Koch, G. Schackert, and M. Kirsch, "Intraoperative imaging of cortical cerebral perfusion by time-resolved thermography and multivariate data analysis," *Journal of Biomedical Optics*, vol. 16, no. 1, pp. 016 001–016 001–6, 2011. [Online]. Available: +http://dx.doi.org/10.1117/1.3528011

[3] A. Gorbach, J. D. Heiss, L. Kopylev, and E. H. Oldfield, "Intraoperative infrared imaging of brain tumors," *Journal of Neurosurgery*, 2004.

[4] P. Branemark, S. Fagerberg, L. Langer, and J. Soderbergh, "Infrared thermography in diabetes mellitus," *Diabetologia*, 1967.

[5] P. Sun, H. Lin, S. Jao, Y. Ku, R. Chan, and C. Cheng, "Relationship of skin temperature to sympathetic dysfunction in diabetic at-risk feet," *Diabetes Research and Clinical Practice*, 2006.

[6] R. Cesaris, A. Grimaldi, M. Balestrazzi, G. Ranieri, R. Chirappa, and F. Avantaggianto, "Changes in blood pressure and thermographic values resulting from use of a beta- blocker plus diuretic and of an alpha-betablocker plus diuretic," *Drugs Under Experimental and Clinical Research*, 1985.

[7] B. Gratt, S. Graff-Radford, V. Shetty, W. Solberg, and E. Sickles, "A six year clinical assessment of electronic facial thermography," *Dentomaxillofacial Radiology*, 1996.

[8] F. Ring, "Pandemic: thermography for fever screening of airport passengers," *Thermology International*, 2007.

[9] V. P. Vavilov, "Dynamic thermal tomography: Recent improvements and applications," *NDT & E International*, 2015.

[10] Z. S. Deng and J. Liu, "Enhancement of thermal diagnostics on tumors underneath the skin by induced evaporation," *Proc. 27th Annual Conference of IEEE Engineering in Medicine and Biology*, 2005.

[11] H. H. Pennes, "Analysis of tissue and arterial blood temperatures in the resting human forearm," *Journal of Applied Physiology*, 1948.

[12] G. Gutierrez and M. Giordano, "Study of the bioheat equation using monte carlo simulations for local magnetic hyperthermia," *Proc. ASME 2008 International Mechanical Engineering Congress and Exposition*, 2008.

[13] A. Nowakowski, *7. Quantitative active dynamic thermal IR-imaging and thermal tomography in medical diagnostics*. Taylor and Francis, 2013.

[14] L. Ye and E. Keogh, "Time series shapelets: A new primitive for data mining," *SIGKDD*, 2009.

[15] W. Gilks, S. Richardson, and D. Spiegelhalter, *Markov Chain Monte Carlo in Practice*. CRC Press, 1995.

[16] C. M. Bishop, *Pattern Recognition and Machine Learning*. Springer, 2006.

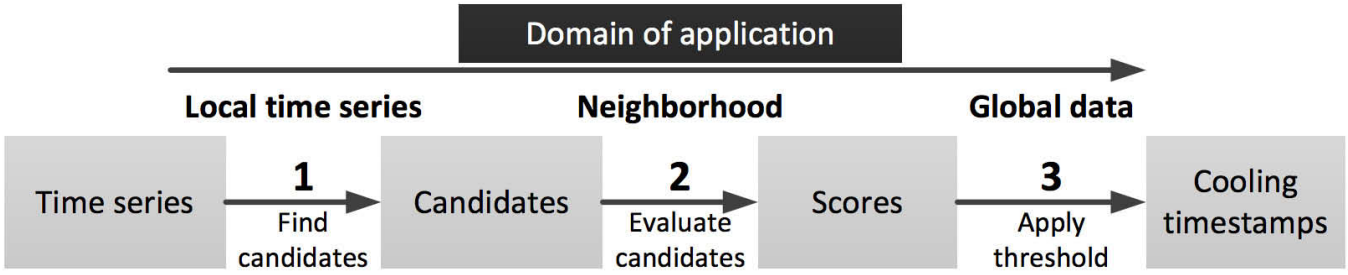

Fig. 1. Overview of the proposed irrigation detection framework.

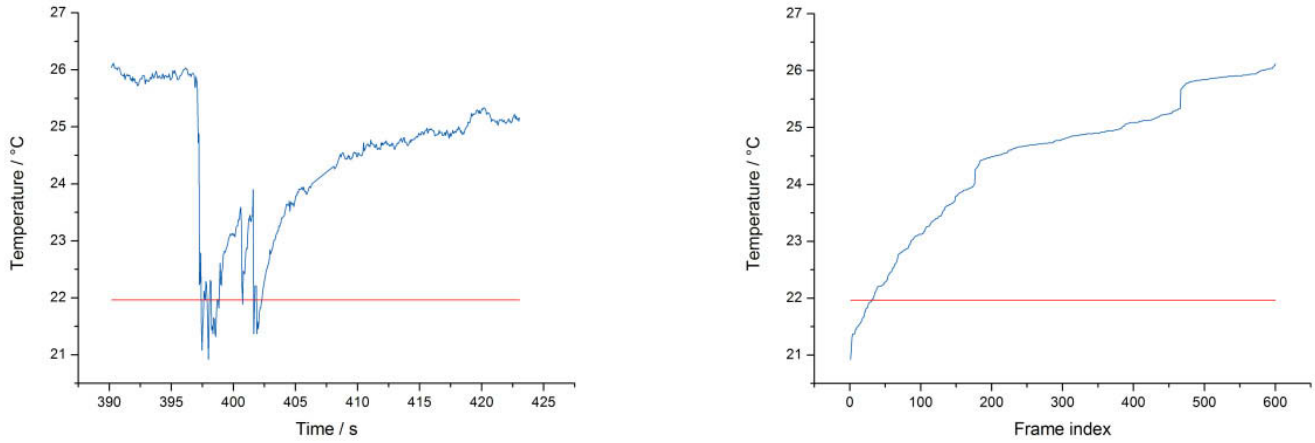

(a) (b)

Fig. 2. **(a)** Temperature time series after application of multiple NaCl irrigations **(b)** The sorted time series shows a characteristic pattern invariant to the number of irrigations.

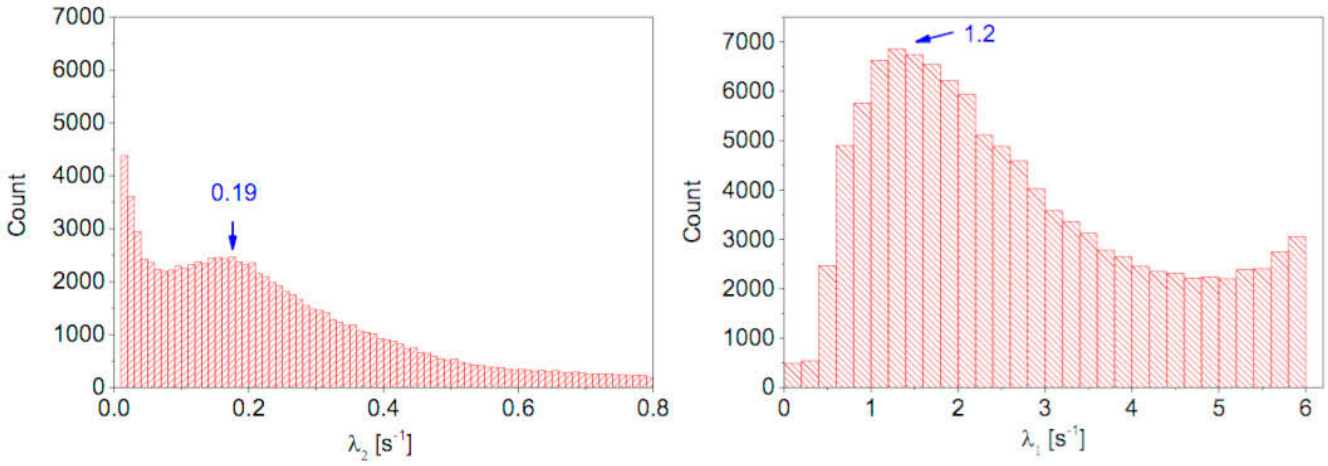

Fig. 4. In our experiments we also validated the model assumption that the time constants of tissue dynamics (left) λ_2 and fluid drainage (right) λ_1 can be separated by application of a large enough temperature gradient.

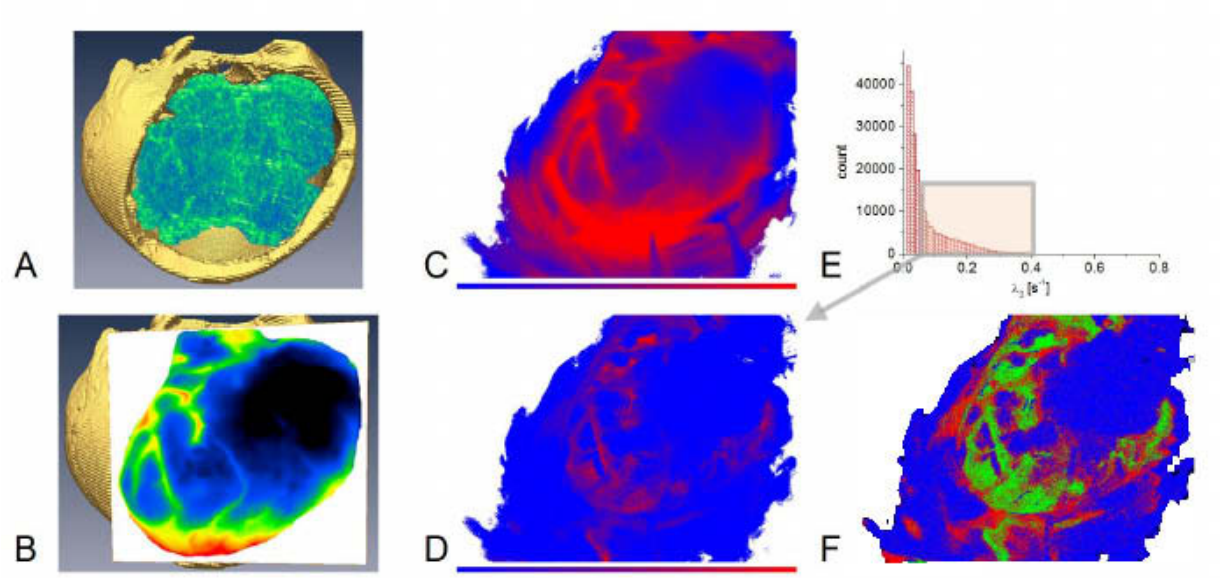

Fig. 5. This figure shows the results of case 5. In **A**, the infarct demarcation is segmented as green-blue in a post-operative CT recording. Subimage **B** shows the orientation of the thermal image to the CT dataset. **C** depicts the temperature distribution at equilibrium temperature after the irrigation. **D** displays the spatial distribution of λ_2 and **E** shows the histogram of all λ_2 values. **F** represents the segmentation as result of fitting the 3-Gaussian mixture model. Blue represents the ischemic / low perfusion state, green the healthy state and red representing uncertainty. The estimated underperfused tissue state strongly correlates with post-operative infarct demarcation. Some tissue is located near well perfused arteries (green) and might indicate areas that might be affected by further ischemic progression. Compared to the raw temperature image of **B** the results allow inferring more detailed information regarding the tissue perfusion.

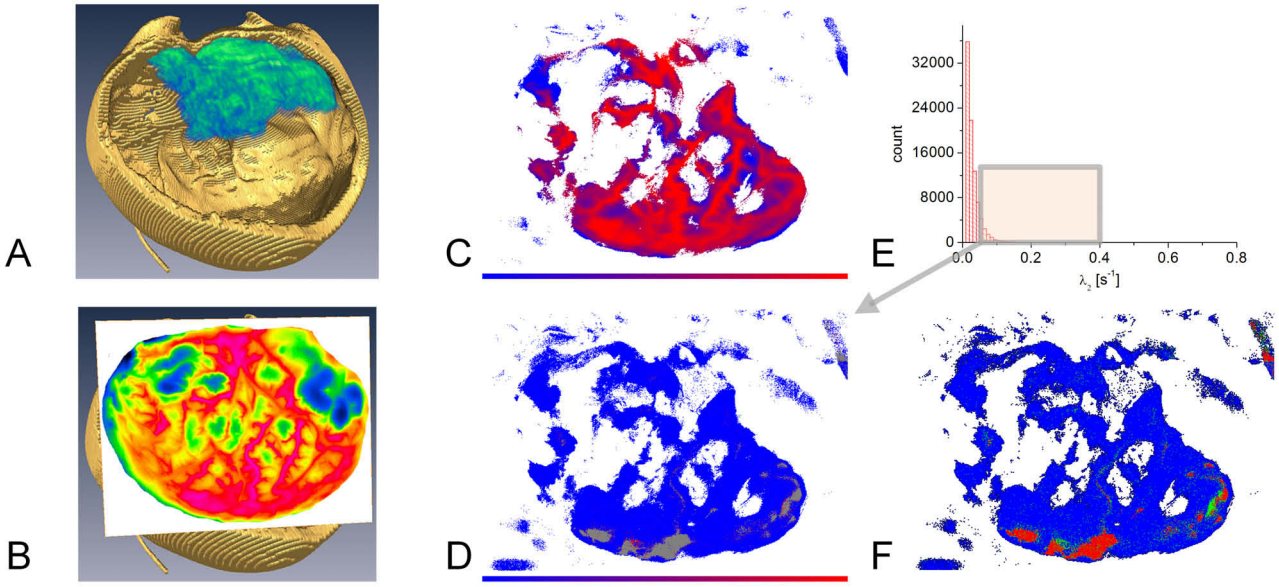

Fig. 6. In case 2, the applied liquid was partially hotter than the surface preventing meaningful results. The cause of this issue was the applied NaCl solution being partially hotter than the surface. Future investigations should therefore consist of a mechanism to provide NaCl liquid at constantly low temperature (e.g. $20°C$). **A** resembles the segmented infarct demarcation while **B** shows the orientation of the thermal image with respect to the CT dataset. In **C**, the equilibrium temperature after the irrigation event with white pixels resembling rejected detections is imaged. **D** displays the spatial distribution of λ_2 and **E** shows the histogram of all λ_2 values. **F** represents the segmentation as result of fitting the 3-Gaussian mixture model.